Exit chart applied to frequency domain turbo equalization for single carrier space-time block code per block

Patricia Isabel Armando Mazeika, Karine Amis Cavalec, Dominique Leroux

EXIT chart applied to frequency domain turbo equalization for single carrier space-time block code per block

Patricia Armando, Karine Amis and Dominique Le Roux
GET-ENST Bretagne, Signal and Communication Department/TAMCIC CNRS UMR 2872
Technopôle Brest-Iroise, CS 83818, 29238 Brest Cedex 3, France
Email: patricia.armando@enst-bretagne.fr, karine.amis@enst-bretagne.fr and dominique.leroux@enst-bretagne.fr

Abstract

This paper is focused on the study of the convergence of the frequency domain turbo equalizer for space-time encoded signals with single-carrier modulation. For this study we employ the extrinsic information transfer chart. We use space-time coding schemes adapted to frequency-selective channels and an efficient generalized receiver based on a space-time frequency domain detector. We study the influence of the orthogonal space-time code per block defined for 2 and 4 transmit antennas in the EXIT chart. Simulation results show that the scheme performs efficiently, for convolutional codes of memory 2, 3 and 5, over frequency-selective block fading channels for the second iteration and beyond.

1 Introduction

Multiple-input multiple-output (MIMO) techniques promise high data rate and robust communications. One technique used in MIMO is known as space-time coding. These codes have become a subject of interest in the research field. In [1] a space-time block code (STBC) for two transmit antennas is introduced. However it assumes flat fading channels, and its generalization for higher antenna numbers is proposed in [2, 3]. The adaptation of these codes to frequency-selective fading channels is presented in [4, 5]. A generalization on the construction of these codes and a generalized maximum likelihood (ML) detector were introduced in [6].

Almost all communication systems suffer from inter-symbol interference (ISI) as a result of frequency-selective fading channel. The BCJR [7] is an optimal receiver based on the known maximum *a posteriori* criterion. Its disadvantage is that its complexity grows up exponentially with the memory of the channel. A nearly optimal receiver for single-input single-output is proposed in [8] based on a linear equalizer (LE), known as turbo minimum mean square error interference cancellation (MMSE-IC-LE). This receiver exploits the contribution of the multipaths followed by the same symbol, canceling at the same time the interference generated by the undesirable symbols.

The convergence of the MMSE-IC-LE was first studied in [9]. The extrinsic information exchanged between the equalizer and the decoder provides the extrinsic information transfer (EXIT) chart and consequently the point of convergence of the turbo equalizer (TE). The convergence is obtained when the two saturation points (intersection point between both traces) come close enough together that they progressively become indistinguishable. The exchange of extrinsic information is then visualized as a stair decoding trajectory in the EXIT chart. The number of steps plotted in the EXIT chart correspond to the number of iterations required for the MMSE-IC-LE to converge.

This paper is focused on the study of the convergence by the EXIT chart of the frequency domain (FD) MMSE-IC-LE introduced in [10]. We use the orthogonal STBC per block (OSTBCB) proposed in [6], and its FD-ML-detector as well. The output when implementing the OSTBCB FD-ML-detector [6] is equivalent to a single-input single-output system. The advantage of our method is that it can be applied to any OSTBCB code of any configuration regarding number of antennas. This model allows the construction of the EXIT chart in the same way as for a single-input single-output system. In addition, our EXIT chart analyzes FD-TE. Furthermore, few references have studied the STBC EXIT chart [11–13] and even less have considered FD-TE OSTBCB EXIT chart [14]. In addition, all references have only considered 2 transmit antennas. We extend our study to 4 transmit antennas and it can be also performed for a higher number thanks to the generalized OSTBCB construction and FD-ML-detector of [6]. Simulation results show that the scheme performs efficiently over frequency-selective block fading channels starting from the second iteration for convolutional codes (CC) of memory 2, 3 and 5. Furthermore, the results confirm that the EXIT chart is a powerful tool to optimize our OSTBCB FD-MMSE-IC-LE.

This paper is organized as follows: Section 2, we start presenting the notations, the system model and the ML detector. Then the FD generalized TE based on the MMSE criterion for OSTBCB is introduced. In Section 3, the EXIT chart is explained. In Section 4 simulations show

the receiver efficiency over frequency-selective block fading channels. Finally, the conclusions are drawn in Section 5.

2 System model

2.1 Orthogonal frequency STBC per block

We consider the OSTBCB of [6, 10], represented in Figure 1. At the transmitter the incoming input bit stream $\{d(n)\}$ is encoded by a forward error correction (FEC) code. A random interleaver Π shuffles the resulting coded data sequence, $c(n) = 0, 1$. Each packet of m coded and interleaved bits is mapped onto an M-ary complex symbol with variance σ_s^2 which belongs to signal set $\mathcal{S}$, where s represents a symbol of the set. The symbols $\{s(n)\}$ are split into K packets of size P denoted $\mathbf{s}_k = \big[s_k(0) \quad .... \quad s_k(P-1)\big], 1 \leq k \leq K$.

Figure 1: Discrete-time equivalent transmitter model

The transmitted symbols are distributed between the n_T transmit antennas by a matrix $\mathrm{c_{ST}}$ of size $T \times n_T$, defined by

$$\mathrm{c_{ST}} = \sum_{k=1}^{K} [\mathbf{s}_k(n)]^{\mathrm{T}} \otimes \beta_{\mathrm{k}}^{-} + [\mathbf{s}_k{}^{\star}(p_n)]^{\mathrm{T}} \otimes \beta_{\mathrm{k}}^{+} \quad (1)$$

where $[\mathbf{a}]^{\star}$ denotes the conjugate of $[\mathbf{a}]$, $[\mathbf{a}]^{T}$ its transpose matrix, $(p_n) = (P-n)\mathrm{mod}(P)$, $\otimes$ represents the Kronecker (tensor) product, and β_{k}^{-} and β_{k}^{+} are $T \times n_T$ complex characteristic matrices of the considered OSTBCB which properties are given in [3].

Let us consider the frequency properties of the OSTBCB given in [6], and let $\mathbf{S}_k(p)$ be the *p-th* coefficient of the P-FFT of $\{\mathbf{s}_k(n)\}$. The P-FFT applied to $\mathrm{c_{ST}}$ along the time dimension (vertical) leads to P complex matrices $C_{ST}(p)$ of size $T \times n_T$ [6]

$$\mathrm{C_{ST}}(p) = \sum_{k=1}^{K} S_k(p)\beta_k^{-} + S_k^{\star}(p)\beta_k^{+}, \; 0 \leq p \leq P-1 \quad (2)$$

Subsequently, each transmitted block is preceded by a cyclic prefix CP which is the repetition of the last G samples of each block. These CPs guarantee circular convolution in the time-domain, *i.e.* a scalar product in the FD. The length of the CP is at least equal to the channel ISI in order to avoid the inter-block interference (IBI).

Assuming perfect carrier and time synchronizations, the received samples $\{y_j(n)\}$ on the receive antenna j can be expressed as

$$y_j(n) = \sum_{i=1}^{n_T} \sum_{l=0}^{L-1} h_{j,i}(n-l) c_{\mathrm{ST}}^{i}(n) + \phi_j(n) \quad (3)$$

where $\{h_{j,i}(n)\}$ are the coefficients of the channel impulse response between transmit antenna i and receive antenna j, $c_{\mathrm{ST}}^{i}(n)$ corresponds to the *m-th* OSTBCB element sent from the *i-th* transmit antenna and $\phi_j(n)$ are complex circular AWGN noise coefficients on received antenna j with zero mean and variance σ_ϕ^2.

After eliminating the CP, $\{y_j(n)\}$ is split into T packets of length P. Then, a P-FFT is applied on each block to obtain the P matrices $Y(p)$ of size $T \times n_R$.

$$\mathrm{Y(p)} = \mathrm{H(p)C_{ST}(p)} + \Phi(p) \quad (4)$$

where $\{\Phi(p)\}$ denotes the P-FFT of the noise $\{\phi(n)\}$, $\mathrm{H(p)} = \{H_{j,i}(p)\}$ with $1 \leq i \leq n_T$, $1 \leq j \leq n_R$ and $\{H_{j,i}(p)\}$ is the P-FFT of the time channel impulse response coefficients $\{h_{j,i}(n)\}$, with $H_{j,i}(p) = \sum_{n=0}^{P-1} h_{j,i}(n) exp(-j2\pi \frac{np}{P})$.

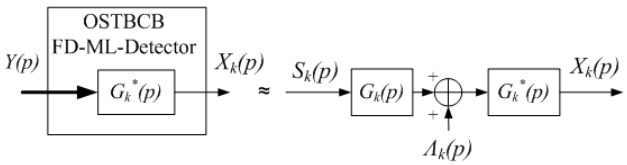

Figure 2: Iterative receiver model for a generic equalizer-decoder scheme

At the receiver, we use the equivalent model of Figure 2. It provides the soft decision variables $X_k(p)$ for each $S_k(p)$ resulting from the application of the maximum likelihood criterion [6]. The soft decisions variables can be described by

$$X_k(p) = G_k^{\star}(p)[G_k(p)S_k(p) + \Lambda_k(p)] \quad (5)$$

where $G_k^{\star}(p)G_k(p) = \mathrm{Tr}[\mathrm{H(p)}^{\dagger}\mathrm{H(p)}]$, $\mathrm{H}^{\dagger}$ denotes the Hermitian of H and $\Lambda_k(p)$ is the equivalent complex AWGN of variance $\sigma_\Lambda^2 = \sigma_\Phi^2 = P\sigma_\phi^2$. Let us denote $B_k(p) = G_k^{\star}(p)\Lambda_k(p)$. Its variance is defined by $\sigma_B^2 = P|G_k(p)|^2\sigma_{\phi_k}^2$.

2.2 Frequency domain MMSE turbo equalization IC-LE [10]

We consider the finite-length MMSE interference cancellation structure of [10] represented in Figure 3. After the P-FFT, the FD-ML-detector detailed in [6] provides $X_k(p)$. Using the equivalent model [8] and the FD-MMSE-IC-LE described in [8] and [15] for single-input single-output systems, an interference cancellation structure consisting of a feed-forward filter $F_k(p)$ and a feedback filter $Q_k(p)$ delivers the estimated symbols $Z_k(p)$ define as

$$Z_k(p) = F_k(p)X_k(p) - Q_k(p)\bar{X}_k(p) \quad (6)$$

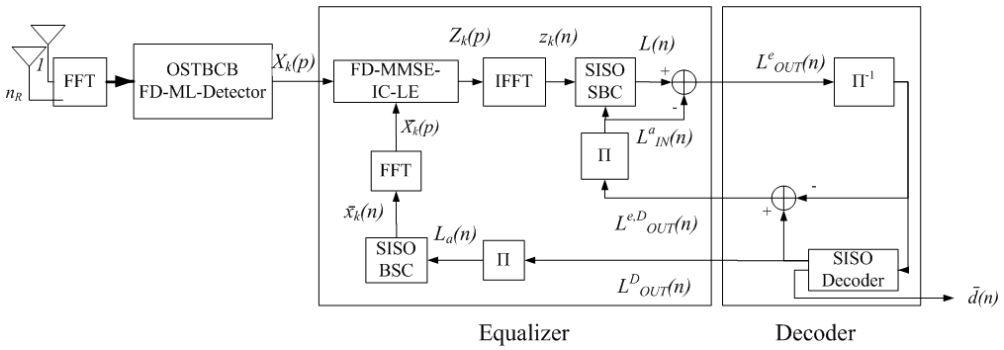

Figure 3: Frequency domain turbo equalizer structure

where $\{\bar{X}_k(p)\}$ is the estimated ISI, $Q_k(p)$ is computed minimizing the mean square error $\varepsilon_{\mathrm{LE}} = \mathrm{E}[|z_k(n) - s_k(n)|^2]$ and $\{z_k(n)\}$ is the IFFT $Z_k(p)$. Due to the FFT properties and assuming *i.i.d.*[1] of $\{s_k(n)\}$, minimizing $\varepsilon_{\mathrm{LE}}$ is equivalent to minimizing each $\mathrm{E}[|Z_k(p) - S_k(p)|^2]$ under the constraint $\sum_{p=0}^{P} Q_k(p) = 0$ *i.e.* $q_k(n = 0) = 0$. The Lagrangian resolution of this optimization leads to $Q_k(p) = F_k(p)|G_k(p)|^2 - \mu$,where $\mu = \frac{1}{P}\sum_{q=0}^{P} F_k(q)|G_k(q)|^2$. The FD equalizer coefficients $F_k(p)$ are given by $F_k(p) = \frac{(\sigma_s^2 - \mu\sigma_{\bar{x}}^2)}{|G_k(p)|^2(\sigma_s^2 - \sigma_{\bar{x}}^2) + \sigma_\phi^2}$

The $\{z_k(n)\}$ are used in the soft symbol to bit converter (SBC) to deliver lineary reliability values used as the inputs of the decoder. The decoder feeds the soft-input soft-output (SISO) bit to symbol converter (BSC) with log-likelihood ratios (LLR) denoted $L^D_{OUT}(n)$ or $L_a(n)$ after interleaving.

The SISO BSC block generates soft symbol estimates. They are computed as the expected value of the transmitted symbols, with respect to the *a priori* probabilities derived from the soft value delivered by the decoder at the previous iteration. $\bar{x}_k(n) = E[s_k(n)|L_a(n)]$

Under the assumption of *i.i.d.* transmitted symbols $\{s_k(n)\}$, $\sigma_{\bar{x}}^2 = E[|s_k(n) - \bar{x}_k(n)|^2|L_a(n)]$. Those soft symbol estimates are exploited as *a priori* information to cancel the ISI in the MMSE-IC-LE.

The output of the SBC denoted $L(n)$ [15] is equal to

$$L(n) = \ln \frac{\sum_{(s\in\mathcal{S}|c^i(n)=1)} Pr(z_k(n)|s_k(n)=s)P_{a,n}(s)}{\sum_{(s_\in\mathcal{S}|c^i(n)=0)} Pr(z_k(n)|s_k(n)=s)P_{a,n}(s)} \quad (7)$$

$$\Pr(z_k(n)|s_k(n)=s) = \frac{1}{\pi\sigma_b^2} e^{-\frac{|z_k(n)-\mu s_k(n)|^2}{\sigma_b^2}} \quad (8)$$

$$P_{a,n}(s) = \prod_{i=1}^{m} P_{a,n}(c_n^i) = \prod_{i=1}^{m} \frac{e^{\frac{(2c_n^i-1)L^a_{IN}(n)}{2}}}{e^{\frac{L^a_{IN}(n)}{2}} + e^{-\frac{L^a_{IN}(n)}{2}}} \quad (9)$$

with $\sigma_b^2 = \mu(\mu-1)\sigma_s^2$ and $\{c_n^i\}_{\{1\le i\le m\}}$ the interleaved encoded bit values mapped to $s \in \mathcal{S}$.

[1] independent and identically distributed

The $L(n)$ values are used to obtain the extrinsic information $L^e_{out}(n)$ [15] defined by

$$L^e_{OUT}(n) \quad = L(n) - L^a_{IN}(n) \quad (10)$$

The SISO decoder provides the *a posteriori* LLRs on the coded bits L^D_{OUT}, defined as follows

$$L^D_{OUT}(c^i(n)) = ln\frac{Pr(c^i(n)=1)|L_a(c^i(n))}{Pr(c^i(n)=0)|L_a(c^i(n))} \quad (11)$$

3 EXIT chart

3.1 EXIT chart applied to OSTBCB

At the receiver after applying the FFT and the OSTBC FD-ML-detector, the system can be modeled as an equivalent single-input single-output scheme. Moreover, the ISI is exploited by the MMSE-IC-LE. This model can be generalized for a large number of transmit and receive antennas as a result of the OSTBCB FD-ML-detector, this antenna number does not influence the applicability of the EXIT chart firstly introduced in [9].

3.2 EXIT chart principle [9]

In figure 4, we simplify the structure presented in Figure 3 by representing only the equalizer, the decoder and they respective inputs and outputs. The EXIT chart analyzes the mutual information computed from the *a priori* probability density function (*p.d.f.*) and extrinsic LLRs exchanged between the decoder and the equalizer.

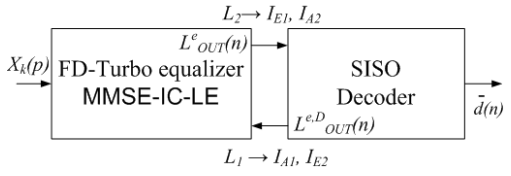

Figure 4: Iterative receiver model for a generic joint equalizer-decoder scheme

Let us assume that the extrinsic information exchanged between the decoder and the equalizer have Gaussian conditional *p.d.f* with mean μ_E and variance $2\mu_E$.

$$f(L_x|c'(n)) = \frac{1}{2\sqrt{\pi\mu_E}} e^{\frac{-(L_x-\mu_E c'(n))^2}{4\mu_E}} \quad (12)$$

where L_x represents the extrinsic information and $c'(n) = 2c(n) - 1$.
We define I_{E1} as the mutual information computed from the transmitted coded bit, $c'(n)$ and the extrinsic information at the equalizer output, L_2. This mutual information depends on the channel, the *a priori* LLRs, L_1 and the E_b/N_0, where E_b is the average energy per transmitted bit and N_0 is the unilateral noise power spectral density. Consequently, I_{A1} is the mutual information calculated from transmitted bit code $c'(n)$ and *a priori* LLRs from the decoder, L_1. Furthermore, I_{E2} denotes the mutual information obtained from the transmit coded bit $c'(n)$ and extrinsic information L_1 at the decoder output. I_{A2} is the mutual information calculated from the transmitted coded bit $c'(n)$ and *a priori* LLRs from the equalizer, L_2. However, the I_{E2} is an entirely depended function of the input L_1. For both inputs (equalizer and decoder), I_A can be calculated as

$$\begin{aligned} I_A = \quad & \tfrac{1}{2} \sum_{c'(n)=\pm 1} \int_{-\infty}^{-\infty} \log_2\left(\tfrac{f(L^A|c'(n))}{f(L^A|-1)+f(L^A|+1)}\right) \\ & \times f(L^A|c'(n))dL^A \end{aligned} \quad (13)$$

And simplified to

$$I_A = 1 - \int_{-\infty}^{\infty} \frac{log_2(1+e^{L^A})}{2\sqrt{\pi\mu_E}} e^{\frac{-(L^A+\mu_E)^2}{4\mu_E}} dL^A \quad (14)$$

The mutual information I_{E1} and I_{E2} are computed employing the approximation given by

$$I_E \backsimeq 1 - E[log_2(1+e^{(-c'(n)L^E)})] \quad (15)$$

The exchange of mutual information between the equalizer and the decoder is visualized as a stair between both mutual information traces (equalizer $\rightarrow$ decoder $\rightarrow$ equalizer), where each step represents the numbers of iterations necessary for the turbo equalizer to converge.

4 Simulation Results

In this section, two MIMO configuration considered. Firstly in Section 4.1, we consider the Alamouti code with 2 transmit antennas and 1 receive antenna ($n_T = 2, n_R = 1$) and secondly in Section 4.1 $n_T = 4, n_R = 1$ is contemplated. In both MIMO configuration, the interleaved data is QPSK modulated.. The FEC code is a $1/2$ rate convolutional code. We consider tree generator polynomials CC$(5,7)_8$, CC$(13,15)_8$ and CC$(171,133)_8$. The total average transmitted power is normalized to unity. The frequency selective channel consists of 5 *i.i.d.* paths of equal average power such that the total average received power is equal to one (EQ-5). $h_{j,i}(l)$ is a complex Gaussian random variable of zero mean and variance $\frac{1}{5}$. We further assume that the channel coefficients are spatially uncorrelated and remain constant during the transmission of one OSTBCB. At the receiver, we assume perfect channel state information and perfect synchronization. In our simulations, 3 iterations of the turbo equalizer are considered. The outer decoder is a BCJR decoder [7].

4.1 EXIT chart validation ($n_T = 2, n_R = 1$)

The OSTBCB considered is derived from the Alamouti scheme and is defined by

$$\mathrm{c} = \begin{bmatrix} \mathbf{s}_k(n) & -\mathbf{s}^{\star}_{k+1}(p_n) \\ \mathbf{s}_{k+1}(n) & \mathbf{s}^{\star}_k(p_n) \end{bmatrix} \quad (16)$$

The EXIT chart of the turbo equalizer is plotted in Figure 5(a). The equalizer characteristics are presented for E_b/N_0 values ranging from 0 dB (bottom) to 5 dB (top) in steps of 1 dB. The decoder characteristics are traced. We can note that the number of iterations required for the convergence of the turbo equalizer IC-LE is equal to two for E_b/N_0 values of 3, 4 and 5 dB. In figure 5(b), we have the I_{E1} as a function of BER. For a BER of 4.10^{-4} the necessary I_{E1} is equal to 0.8 and the number of iterations of the turbo equalizer is also 2 in order to achive convergence.

In Figure 5(c), the BER is given as a function of E_b/N_0 with a pseudo random interleaver of length 1024. The genie equalizer and the decoder bounds (obtained with perfect ISI knowledge at the equalizer and SBC input) are plotted as references. The SBC and the decoder output BERs are given for the first to the third iteration. In comparison with the first iteration, the third iteration exhibits a gain of 1.5 dB for a BER of 2.10^{-2} (resp. 1 dB for a BER of 2.10^{-4}) at the SBC output (resp. decoder output). Moreover the equalizer achieves the genie equalizer bound after 2 iterations and the decoder performs at 0.2 dB of the genie decoder bound. One can check that the genie bound match with the theoretical bit error probability of a QPSK modulated SISO system over the Rayleigh frequency-selective fast fading channel with $n_T \times L$ taps [16]. From Figure 5(c), we note that at the second iteration the maximum gain of the turbo equalizer is almost achieved which confirms the number of iteration obtained with the EXIT chart of figure 5(a). Figure 5(d) is a zoomed version of Figure 5(a), we can observe a third little step that represents one third iteration which is the convergence gain between the second and the third iteration. This little gain can be also noticed in Figure 5(c) between the second and third iteration. The EXIT chart for the tree convolutional codes (CC(5,7), CC(13,15) and CC(133,171)) is plotted in Figure 6(a). We notice that the number of iterations is about 2 for the 3 convolutional codes.

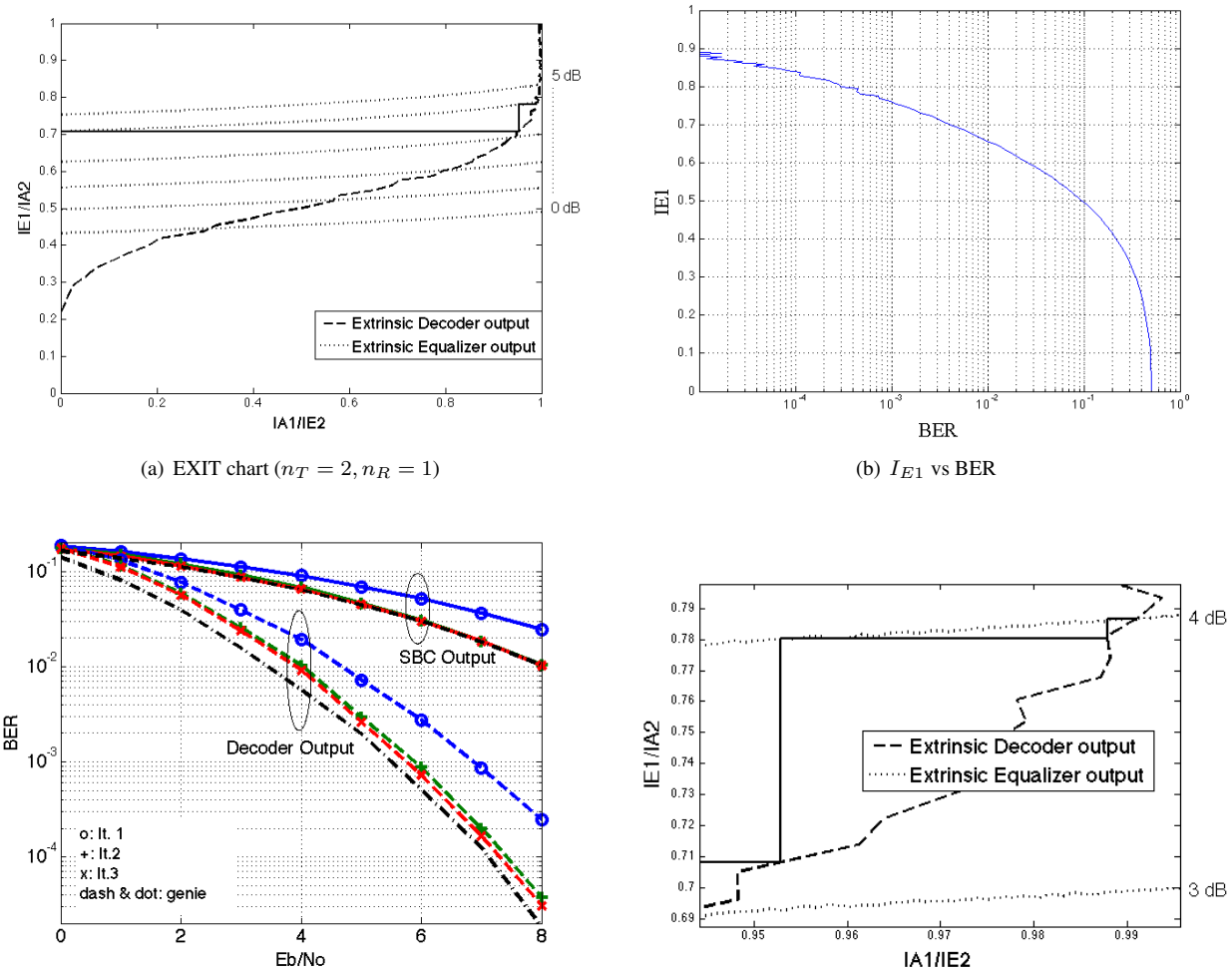

(a) EXIT chart ($n_T = 2, n_R = 1$)

(b) I_{E1} vs BER

(c) BER vs E_b/N_0

(d) Zoom

Figure 5: EXIT chart and performance for MMSE-IC-LE turbo equalizer, OSTBCB ($n_T = 2, n_R = 1$) with QPSK over the EQ-5 block fading channel

4.2 EXIT chart validation ($n_T = 4, n_R = 1$)

We consider the OSTBC proposed in [17] for $n_T = 4$ and applying (2) we obtain (17). In Figure 6(b) is plotted the EXIT chart for QPSK modulated signal. The extrinsic coder information is considered for the 3 convolutional codes represented in Figure 6(a). We can observe that the genie extrinsic equalizer mutual information have the same mean such as the configuration ($n_T = 2, n_R = 1$) *i.e.* Figure 6(a). However the genie extrinsic equalizer mutual information is not the same for both MIMO configuration. To any E_b/N_0, we can note that in the configuration ($n_T = 4, n_R = 1$) the difference between the first I_{E1} and the last I_{E1} is smallest than the first I_{E1} and the last I_{E1} in the configuration ($n_T = 2, n_R = 1$). The difference can be related to the gain in space diversity introduced by the higher number of antennas of the configuration ($n_T = 4, n_R = 1$). The number of iterations to converge is also about 2. However, the gain between the second and the thirst iteration is almost impercetible. Moreover, this results are confirmed using the BER *vs* E_b/N_0.

$$\mathrm{c} = \begin{bmatrix} \mathbf{s}_k(n) & \mathbf{s}^{\star}_{k+1}(p_n) & \frac{\mathbf{s}_{k+2}(n)}{\sqrt{2}} & \frac{\mathbf{s}_{k+2}(n)}{\sqrt{2}} \\ -\mathbf{s}^{\star}_{k+1}(p_n) & \mathbf{s}^{\star}_{k}(p_n) & \frac{\mathbf{s}_{k+2}(n)}{\sqrt{2}} & \frac{\mathbf{s}_{k+2}(n)}{\sqrt{2}} \\ \frac{\mathbf{s}^{\star}_{k+2}(p_n)}{\sqrt{2}} & \frac{\mathbf{s}^{\star}_{k+2}(p_n)}{\sqrt{2}} & \frac{-\mathbf{s}_k(n)-\mathbf{s}^{\star}_k(p_n)+\mathbf{s}_{k+1}(n)-\mathbf{s}^{\star}_{k+1}(p_n)}{2} & \frac{\mathbf{s}_k(n)-\mathbf{s}^{\star}_k(p_n)-\mathbf{s}_{k+1}(n)-\mathbf{s}^{\star}_{k+1}(p_n)}{2} \\ \frac{\mathbf{s}^{\star}_{k+2}(p_n)}{\sqrt{2}} & \frac{\mathbf{s}^{\star}_{k+2}(p_n)}{\sqrt{2}} & \frac{\mathbf{s}_k(n)-\mathbf{s}^{\star}_k(p_n)+\mathbf{s}_{k+1}(n)+\mathbf{s}^{\star}_{k+1}(p_n)}{2} & \frac{-\mathbf{s}_k(n)-\mathbf{s}^{\star}_k(p_n)-\mathbf{s}_{k+1}(n)+\mathbf{s}^{\star}_{k+1}(p_n)}{2} \end{bmatrix} \tag{17}$$

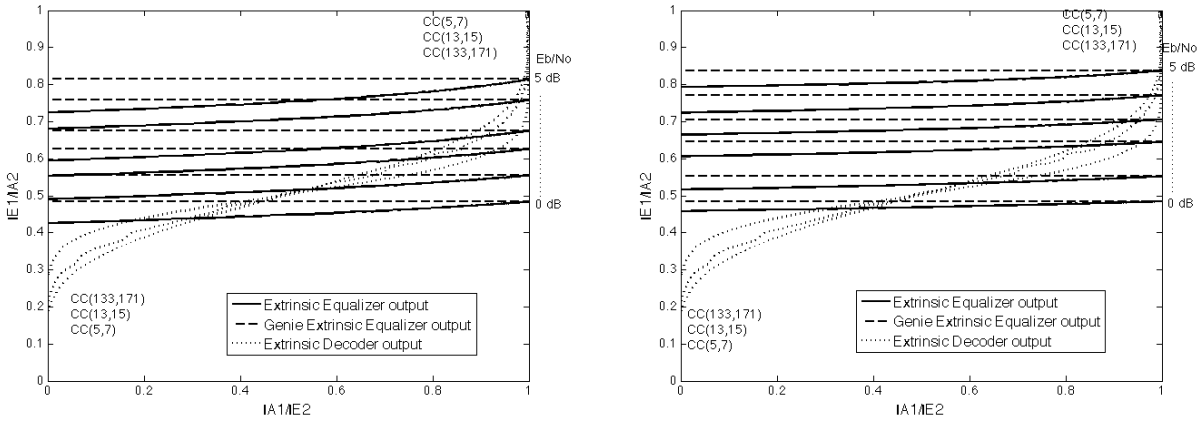

(a) $n_T = 2, n_R = 1$ (b) $n_T = 4, n_R = 1$

Figure 6: EXIT chart applied to MMSE-IC-LE turbo equalizer, OSTBCB with QPSK CC(13,15) over the EQ-5 block fading channel

5 Conclusions

In this paper we have applied the EXIT chart to study the convergence of the generalized turbo equalizer structure presented in [10] for the generalized OSTBCB proposed in [6]. Simulations carried out over a multipath block fading channel have shown the efficiency of the proposed receiver. Furthermore, the EXIT chart makes easy the optimization of the turbo equalizer structure, such as the choice of the mapping and the E_b/N_0 threshold for a target BER.

References

[1] S. M. Alamouti, "A simple transmit diversity technique for wireless communications," *IEEE Journal on Select. Areas in Commun.*, vol. 16, pp. 1451–1458, Oct. 1998.

[2] V. Tarokh, H. Jafarkhani, and A. Calderbank, "Space-time block codes from orthogonal designs." *IEEE Trans. Infor. Theory*, vol. 45, no. 5, pp. 1456–1467, Jul. 1998.

[3] O. Tirkkonen and A. Hottinen, "Square-matrix embeddable space-time block codes for complex signal constellations," *IEEE Trans. Infor. Theory*, vol. 48, no. 2, pp. 384–395, Feb. 2002.

[4] IEEE, "IEEE standard for local and metropolitan area networks: Air interface for fixed broadband wireless access system," *IEEE Std.802.16*, 2001.

[5] E. Lindskogand A. Parogyaswami, "A transmit diversity scheme for channels with intersymbol interference," *IEEE International Conference on Communication.*, pp. 307–311, Jun. 2000.

[6] K. Amis and D. Le Roux, "Predictive decision feedback equalization for space-time block codes with orthogonality in frequency domain," *PIMRC'05*, pp. 1140–1144, Sep. 2005.

[7] L. Bahl, J. Cocke, F. Jelinek, and J. Raviv, "Optimal decoding of linear codes for minimizing symbol error rate." *IEEE Trans. on Inform. Theory*, vol. 20, pp. 284–287, March 1974.

[8] C. Laot, R. Le Bidan, and D. Le Roux, "Low complexity linear turbo equalization: A possible solution for EDGE." *IEEE Trans. Wireless Commun.*, vol. 4, pp. 965–974, May. 2005.

[9] S. ten Brink, "Convergence of iterative decoding," *Electronics Letters.*, vol. 35, no. 13, pp. 1117–1119, Jun. 1999.

[10] P. Armando, K. Amis, and D. Le Roux, "Frequency-domain turbo equalization for single carrier space-time block code per block," *PIMRC'07*, Sep. 2007.

[11] P. Xiao, R. Carrasco, and I. Wassel, "EXIT chart analysis of space-time turbo equalizer," *IEEE ITW'06*, 2006.

[12] A. Sezgin, D. Wübben, R. Böhnke, and V. Kühn, "EXIT-chart for space-time block codes," *ISIT*, Jul. 2003.

[13] L. Zhao and J. Huber, "A new high power efficient bit-interleaved concatened STBC," *VTC*, 2003.

[14] L. Dong and Y. Zhao, "Frequency-domain turbo equalization for single carrier mobile systems," *MILCOM'06*, 2006.

[15] R. Le Bidan, "Turbo-equalization for bandwidth-efficient digital communications over frequency-selective channels." Ph.D. dissertation, INSA de Rennes, 2003.

[16] P. Armando, K. Amis, and D. Le Roux, "SINR comparison of single carrier and OFDM orthogonal space-time block coded transmissions," *submitted to VTC'08*, May. 2008.

[17] V. Tarokh, H. Jafarkhani, and A. Calderbank, "Space-time block coding for wireless communications: performance results," *IEEE Journal on Select. Areas in Commun.*, vol. 17, March 1999.